MOLECULAR AND CELLULAR BIOLOGY, May 2006, p. 3595–3609 Vol. 26, No. 9
0270-7306/06/$08.00+0 doi:10.1128/MCB.26.9.3595–3609.2006

Loss of *TSLC1* Causes Male Infertility Due to a Defect at the Spermatid Stage of Spermatogenesis†

Louise van der Weyden,[1] Mark J. Arends,[2] Oriane E. Chausiaux,[3] Peter J. Ellis,[3] Ulrike C. Lange,[4] M. Azim Surani,[4] Nabeel Affara,[3] Yoshinori Murakami,[5] David J. Adams,[1] and Allan Bradley[1]*

Mouse Genomics Lab, Wellcome Trust Sanger Institute, Wellcome Trust Genome Campus, Cambridge, United Kingdom[1]; Department of Pathology, University of Cambridge, Addenbrooke's Hospital, Cambridge, United Kingdom[2]; Human Molecular Genetics Group, Department of Pathology, University of Cambridge, Tennis Court Road, Cambridge, United Kingdom[3]; Wellcome Trust/Cancer Research UK Gurdon Institute, The Henry Wellcome Building of Cancer and Developmental Biology, Tennis Court Road, Cambridge, United Kingdom[4]; and Tumor Suppression and Functional Genomics Project, National Cancer Center Research Institute, Tokyo, Japan[5]

Received 5 August 2005/Returned for modification 1 October 2005/Accepted 30 January 2006

Tumor suppressor of lung cancer 1 (TSLC1), also known as SgIGSF, IGSF4, and SynCAM, is strongly expressed in spermatogenic cells undergoing the early and late phases of spermatogenesis (spermatogonia to zygotene spermatocytes and elongating spermatids to spermiation). Using embryonic stem cell technology to generate a null mutation of *Tslc1* in mice, we found that *Tslc1* null male mice were infertile. *Tslc1* null adult testes showed that spermatogenesis had arrested at the spermatid stage, with degenerating and apoptotic spermatids sloughing off into the lumen. In adult mice, *Tslc1* null round spermatids showed evidence of normal differentiation (an acrosomal cap and F-actin polarization indistinguishable from that of wild-type spermatids); however, the surviving spermatozoa were immature, malformed, found at very low levels in the epididymis, and rarely motile. Analysis of the first wave of spermatogenesis in *Tslc1* null mice showed a delay in maturation by day 22 and degeneration of round spermatids by day 28. Expression profiling of the testes revealed that *Tslc1* null mice showed increases in the expression levels of genes involved in apoptosis, adhesion, and the cytoskeleton. Taken together, these data show that Tslc1 is essential for normal spermatogenesis in mice.

The immunoglobulin superfamily (IGSF) is one of four categories of cell adhesion molecules (including the integrins, the selectins, and the cadherins) (21) and consists of cell surface receptors such as neural cell adhesion molecules (NCAMs), intercellular adhesion molecules, and nectins. IGSF members, identified by their characteristic immunoglobulin-like domains, function as adhesion molecules and cell surface recognition molecules involved in various cellular processes, including proliferation, survival, differentiation, and migration (41). Originally known as IGSF4 (immunoglobulin superfamily member 4) (19), TSLC1 has been characterized by several independent research groups, and as a result, this molecule has several names (reviewed in reference 48). IGSF4 was first characterized as a tumor suppressor of non-small-cell lung cancer and termed TSLC1 (tumor suppressor of lung cancer 1) (26, 33). Researchers that found a role for this molecule in adhesion of spermatogenic cells to Sertoli cells termed it a spermatogenic immunoglobulin superfamily member (SgIGSF) (46), and those that revealed a role in driving the synaptic formation of neural cells termed it synaptic cell adhesion molecule (SynCAM) (2). In addition, other names for this molecule include Necl-2 (nectin-like molecule 2) (39) and RA175 (14). Since our interest in IGSF4/TSLC1 is its potential as a lung cancer tumor suppressor gene as well as its involvement in spermatogenesis, we will hereafter refer to the molecule as TSLC1.

TSLC1 is composed of an N-terminal signal sequence and three immunoglobulin-like domains that can interact in a homophilic (28) and heterophilic manner. Only recently has a heterophilic binding partner been identified, namely, class I-restricted T-cell-associated molecule (CRTAM), a receptor primarily expressed on activated cytotoxic lymphocytes (5, 16). TSLC1 also contains a transmembrane domain and a cytoplasmic tail which harbors two important binding motifs, namely, a protein 4.1 binding motif (through which TSLC1 binds the anchoring protein DAL1, which interacts with actin filaments [49]) and a PDZ binding motif (through which TSLC1 binds the PDZ domain-containing proteins CASK and syntenin [2] and MPP3, a human homologue of the *Drosophila* tumor suppressor gene *Dlg* [15]).

Mammalian spermatogenesis involves the differentiation of diploid spermatogonia into spermatocytes and then, through two successive meiotic divisions, into haploid round spermatids. During spermiogenesis, the haploid round spermatids undergo an elongation phase, transforming them into mature spermatozoa. Daughter cells arising from a single spermatogonial stem cell remain connected by cytoplasmic bridges throughout this process, only separating towards the end of spermiogenesis. The process of spermatogenesis is regulated by a variety of hormonal and local factors (9) as well as by direct interaction between spermatogenic cells and Sertoli cells; important structural junctions are formed between the Sertoli cells and spermatogenic

* Corresponding author. Mailing address: Wellcome Trust Sanger Institute, Wellcome Trust Genome Campus, Hinxton, Cambridge CB10 1SA, United Kingdom, Phone: 44-1223-834-244. Fax: 44-1223-494-714. E-mail: abradley@sanger.ac.uk.

† Supplemental material for this article may be found at http://mcb.asm.org/.

cells at different maturation stages (7). In the testis, TSLC1 is strongly expressed in the spermatogenic cells of the seminiferous tubules; TSLC1 is expressed in spermatogenic cells undergoing the early and late phases of spermatogenesis (spermatogonia to zygotene spermatocytes and then elongating spermatids to spermiation), whereas other cell types, including Sertoli cells, lack expression of this protein (47). These findings have led to the hypothesis that TSLC1 functions as a cell adhesion molecule during the early steps of spermatogenesis by binding to a membrane molecule on Sertoli cells in a heterophilic manner.

In view of the spermatogenic phenotype, we have studied *Tslc1* null and conditional knockout mice in order to dissect the functions attributed to Tslc1 in spermatogenesis. We show that *Tslc1* null male mice are completely infertile. They show a defect in maturation at the spermatid stage of spermatogenesis, characterized by spermatids prematurely degenerating with apoptotic cell death and sloughing off into the lumen, with the production of very few spermatozoa that show severe head malformations and are rarely motile. Thus, Tslc1 is essential for normal spermatogenesis in mice.

MATERIALS AND METHODS

Construction of *Tslc1* targeting vector and generation of *Tslc1* mutant mice. To generate the *Tslc1* targeting vector (pAL1), DNA fragments for the 5′, conditional, and 3′ homology arms were amplified from RPCI-21 PAC "456b9" DNA by PCR using Platinum PCR High Fidelity supermix (Invitrogen, San Diego, CA) for 10 to 18 cycles. The homology arms consisted of a 4-kb 5′ arm (containing a portion of intron 8 flanked by AscI sites), a 1-kb conditional arm (containing exon 9 flanked by HindIII sites), and a 4.5-kb 3′ homology arm (containing exon 10 and the 3′ untranslated region flanked by NotI sites), which were cloned into pGEM-T Easy (Promega, Madison, WI), sequenced, and then subcloned into the AscI, HindIII, and NotI sites of pFlexible (45), respectively. A negatively selectable marker, DT-A (50), was then cloned into the PmeI site of pFlexible. Ten micrograms of AvrII-linearized pAL1 was electroporated into 1×10^7 AB2.2 embryonic stem (ES) cells (from mouse strain 129S5/SvEvBrd) (36) and grown with 3 μg/ml puromycin selection. Cells were cultured on a lethally irradiated SNL76/7 feeder layer (30). ES clones were picked into 96-well plates after 9 days of drug selection and expanded, and targeted clones were identified by Southern blot analysis using PCR-amplified probes on StuI- or EcoRV-digested genomic DNA with a 5′ or 3′ external probe, respectively. pAI3 is the 540-bp 5′ external probe (forward, 5′-GGG GGT TGA AGG AGG CTT AGA AGT GCC CCA CTT TAA ATG A-3′; reverse, 5′-CTT TTT CTC CTT GCA TTC ACT CCT TAA ACG CTT AC-3′), and pAJ10 is the 214-bp 3′ external probe (forward, 5′-ACA AAA AAA CTA CCA TTG TTC ACA GAA TTG GCA TCT CAT T-3′; reverse, 5′-ATT ATT ATT TTT CCA ATG TGT GGG GCC TAC ACT TT-3′). The correctly targeted allele was termed *Tslc1*^{Brdm1} (*m1*). To generate null and conditional alleles, a cell line with the *m1* allele (LW1) was electroporated with 10 μg of a Cre-expressing plasmid (pTURBO-Cre; GenBank accession no. AF334827) or an Flpe-expressing plasmid (pFLPe) (38), respectively. After 3 days of culture, the cells were trypsinized, reseeded at 3×10^5 cells/10-cm-diameter plate, and cultured in 0.2 μM FIAU for 5 days. After this time, the cells were grown for a further 3 days in drug-free medium before the resulting colonies were trypsinized, pooled, and analyzed by Southern blotting using the pAJ10 probe on PacI-digested genomic DNA. The allele generated with Flpe, which showed a 7.5-kb fragment, was termed *Tslc1*^{Brdc1} (*c1*; conditional allele), and the allele generated with Cre, which showed a 9-kb fragment, was termed *Tslc1*^{Brdm2} (*m2*; null allele). ES cell clones for the null and conditional alleles were transmitted through the germ line and bred to homozygosity (maintained on a mixed 129/Sv-C57BL/6 background). Mice were housed in accordance with Home Office regulations (United Kingdom).

Genotyping of *Tslc1* mutant mice by genomic PCR. Genomic DNA was amplified in 50-μl reaction mixtures using 45 μl Platinum PCR supermix (Invitrogen) and 100 ng of each primer pair (TSL-5/TSL-3 or TSL-C/TSL-3). The primer sequences were as follows: TSL-3 (reverse primer), 5′-TAC CAG GAG GGG AGA AGA GGC CCA GAG C-3′; TSL-5 (forward primer), 5′-AGC ATC CCT TTC CAC CAT AGT TTT CTC TCT-3′; and TSL-C (forward primer), 5′-AGT CTA CAT TTG GGA ATC AAA ATG GTA AGG-3′. The PCR cycle profile was as follows: 1 cycle at 94°C for 2 min followed by 30 cycles at 94°C for 30 s, 65°C for 1 min, and 72°C for 30 s, with a final cycle of 72°C for 10 min.

Reverse transcription-PCR (RT-PCR). RNAs were extracted from +/+, *c1*/*c1*, and *m2*/*m2* mouse brains (RNAqueous; Ambion, Austin, TX), and 1.5 μg of total RNA was used to generate cDNAs (RETROscript; Ambion). The cDNAs were amplified in 50-μl reaction mixtures using 45 μl Platinum PCR supermix (Invitrogen) and 100 ng of each primer pair with the following PCR cycle profile: 1 cycle at 94°C for 2 min followed by 30 cycles at 94°C for 30 s, 65°C for 1 min, and 72°C for 30 s, with a final cycle of 72°C for 10 min. All PCR products were cloned into pGEM-T Easy and sequenced to confirm their identity. The specific primers used were as follows: for *Tslc1* exons 1 to 3, 5′-GAT ATC CAG AAA GAC ACG GCA GTT GAA GGG G-3′ and 5′-CTT CCC GGG TTA GGC CTT GCA GAG GGT A-3′; for exons 5 to 7, 5′-TCA GAG GTG GAG GAG TGG TCG GAC ATG TA-3′ and 5′-CAT ACA GCA TAT AGT CCG AAT GAG CCT T-3′; for exons 9 and 10, 5′-CTC GAG CAG GTG AAG AGG GGA CCA TTG GG-3′ and 5′-GAT GAA GTA CTC TTT CTT TTC TTC GGA GT-3′; for exons 7 to 10, 5′-AAG GCT CAT TCG GAC TAT ATG CTG TAT GTA T-3′ and 5′-TGC TGC GTC ATC GGC TCC TTT GGC TTC ATG A-3′; and for β-actin gene exons 2 and 3, 5′-ACC AAC TGG GAC GAT ATG GAG AAG A-3′ and 5′-TAC GAC CAG AGG CAT ACA GGG ACA A-3′. For PCR using an oocyte (germinal vesicle stage) cDNA library (a gift from Joanna Maldonado-Saldivia), primers for *Tslc1* exons 1 to 3 and *Oct4* (5′-GAG GAT CAC CTT GGG GTA CA-3′ and 5′-CTC ATT GTT GTC GGC TTC CT-3′) were used with the PCR cycle profile shown above.

Quantitative real-time PCR. The expression of *Cklf1*, *Xmr*, and *Ssty* was examined in testes and epididymides from 3-month-old +/+, +/*m2*, and *m2*/*m2* mice, with the β-actin gene used as a control gene ($n = 2$ for each genotype; the assay was performed in triplicate). Total RNAs were extracted with TRIreagent (Sigma) and cleaned using MinElute columns (QIAGEN, Valencia, CA). RNAs were treated with DNase I before RT-PCR, and 500 ng total RNA was used for each RT-PCR. Real-time RT-PCR was performed in 96-well plates using a QuantiTect SYBR green RT-PCR kit (QIAGEN) according to the manufacturer's protocols, quantifying the resulting fluorescence using an iCycler system (Bio-Rad, United Kingdom). The RT step was done at 50°C for 30 min, followed by incubation at 95°C for 15 min to activate the PCR enzyme. The PCR cycling conditions were 95°C for 15 s, 59°C for 30 s, 72°C for 30 s, and 77°C for 10 s. Real-time fluorescence data were captured during the 77°C step of the cycle (the extra step was necessary to avoid interference from primer dimer signals). Melt curve data were obtained to confirm amplification of the correct product in each well. A crossing-point threshold cycle (C_T) value was obtained for each well as the fractional cycle number at which the measured fluorescence crossed the threshold of 60 units, a value chosen such that all reactions in all plates were in log phase. The average C_T was calculated for each gene in each sample. Data were normalized by reference to β-actin, with ΔC_T calculated as follows: $\Delta C_T = C_{T(\text{test})} - C_{T(\text{actin})}$. $\Delta\Delta C_T$ values were then calculated as the change in ΔC_T for the *m2*/*m2* genotype relative to the wild type. The specific primers used were as follows: for *Cklf1*, 5′-TTTX GAA ACA ATG CTC CCA CA-3′ and 5′-ACC TCC AAG GAA CAC ACA GG-3′; for *Xmr*, 5′-TTC AGA TGA AGA AGA AGA GCA GG-3′ and 5′-TCC ATA TCA AAC TTC TGC TCA CAC-3′; for *Ssty*, 5′-AGA AGG ATC CAG CTC TCT ATG CT-3′ and 5′-CCA GTT ACC AAT CAA CAC ATC AC-3′); and for β-*actin*, 5′-ATC ATG TTT GAG ACC TTC AAC AC′ and 5′-TCT GCG CAA GTT AGG TTT TGT-3′.

Microarray analysis. RNAs for microarray analysis were obtained from the testes of 3-month-old +/+ and *m2*/*m2* mice ($n = 2$ for each genotype). Array hybridizations were performed on the *Mm*cDNAv1 chip, a cDNA microarray representing 11,000 different mouse genes. The clone collection was composed of the NIA 7.4k cDNA set (44), 400 hand-picked clones from the NIA 15k mouse cDNA set (22, 42), and ~8,500 hand-selected clones from eight testis cell-specific and subtracted mouse cDNA libraries (8, 29) (Pathology Department, Centre for Microarray Resources, Cambridge, United Kingdom). cDNA labeling and hybridization to arrays were performed as previously described (11). Technical reproducibility was assessed at two levels, namely, within each slide (duplicate of each clone) and between slides (four technical replicates of the experiment). Signal intensities were quantified using BlueFuse software (BlueGnome Limited, Cambridge, United Kingdom), and the data from duplicates on the slides were fused. This method averages spots from the same array on the basis of the estimated confidence in each ratio and the level of agreement between duplicates. The resulting data were imported into Knowledge Discovery Environment (InforSense Limited, London, United Kingdom), and the data were normalized to the median of overall intensities for the slide. Data from the four technical replicates allowed us to calculate a coefficient of variation for each clone (the quality of the data are inversely related to the coefficient of variation). Data were sorted into 10 equal-width bins based on absolute fluorescence intensities, and

the most variable clones (the 10% with the highest coefficients of variation) in each bin were excluded from further analysis (43). To identify differentially expressed genes, we used an intensity-dependent Z score. This measures the number of standard deviations a particular data point is from the mean relative to other clones expressed at a similar absolute level (35). Clones with ratios of >2 standard deviations from the mean of the window were considered differentially expressed (95% confidence level). Onto-Express (10, 23) was used to classify the differentially expressed genes according to their gene ontology categories.

Histological analysis. For histology, tissues were fixed in 10% neutral buffered formalin and embedded in paraffin. Tissue sections were stained with either hematoxylin and eosin or periodic acid-Schiff stain and examined by light microscopy. For immunohistochemistry, tissues were fixed in 4% paraformaldehyde in phosphate-buffered saline (PBS), embedded in paraffin, sectioned, and stained for Tslc1 using either CC2 (a rabbit polyclonal antibody against the C-terminal 18 amino acids of TSLC1 [24]) or EC2 (a rabbit polyclonal antibody against the extracellular domain of TSLC1 [amino acids 159 to 223] [23]). For cryosections, tissues were fixed in 4% paraformaldehyde in PBS, embedded in optimal-cutting-temperature compound, sectioned, stained for actin using Alexa fluor 568-phalloidin (Molecular Probes) or for cell death using an in situ cell death detection kit (Roche Diagnostics, Indianapolis, IN), and imaged by confocal microscopy. Data from terminal deoxynucleotidyltransferase-mediated dUTP-biotin nick end labeling (TUNEL) counts are based on a total count of 290 tubules per testis. For electron microscopy, tissues were fixed and processed in resin as previously described (1), and transmission electron microscopy was carried out on a Phillips 410LS instrument at 80 kV.

Flow cytometry. Testes were excised from 3-month-old +/+ and *m2*/*m2* mice and gently crushed through 100-μm cell strainers (BD Falcon, Bedford, MA) in PBS before being fixed in 100% ethanol overnight at 4°C. The cells (1.5×10^6) were then treated with RNase A (2 μg/ml; Sigma, St. Louis, MO) for 30 min at room temperature and stained with propidium iodide (50 μg/ml; Sigma), and the DNA content was analyzed by flow cytometry. All fluorescence-activated cell sorting data analysis was performed using WinMDI, version 2.8, software.

Fertility studies. To assess male fertility, +/+ ($n = 6$), +/*m2* ($n = 15$), and *m2*/*m2* ($n = 15$) male mice at 2 to 4 months of age were mated with either +/+ or +/*m2* females of different ages at a ratio of 1:1 or 1:2. To assess female fertility, +/+ ($n = 6$), +/*m2* ($n = 18$), and *m2*/*m2* ($n = 13$) female mice at 2 to 6 months of age were mated with either +/+ or +/*m2* males of different ages at a ratio of 2:1. In both cases, the breeding pairs were maintained for a minimum of 2 months or until a litter was born.

Analysis of spermatozoa. Epididymides were removed from four or five (from each group) +/+, +/*m2*, and *m2*/*m2* male mice at 3 months of age. The cauda region from one epididymis was cut open and incubated in a defined volume of Dulbecco modified Eagle medium with 10% fetal calf serum at 37°C for 10 min to allow dispersion of the contents. A homogeneous suspension was then diluted and spread over a hemacytometer, and the number of mature spermatozoa (those with a head and tail) was counted and expressed as spermatozoa (10^6)/cauda. Motility was defined as the percentage of motile spermatozoa per defined volume.

Measurement of testosterone levels. To assess testosterone levels, whole blood was collected from terminally anesthetized +/+ ($n = 9$), +/*m2* ($n = 4$), and *m2*/*m2* ($n = 10$) male mice at 32 to 36 weeks of age, and sera were isolated by centrifugation at $2{,}000 \times g$ for 20 min. Serum testosterone levels were quantified using a Coat-A-Count free testosterone in vitro diagnostic test kit (Diagnostic Products Corporation, Los Angeles, CA) according to the manufacturer's instructions.

Statistics. For all comparisons, Student's *t* test (unpaired and two-tailed) was used to generate *P* values.

RESULTS

Generation of *Tslc1* null and conditional mice. To assess the physiological role of TSLC1, we have generated null and conditional alleles of the *Tslc1* gene by gene targeting. The targeted locus has *loxP* sites flanking exon 9 and *FRT* sites flanking the selection cassette (Fig. 1A). Exon 9 encodes the transmembrane domain. We reasoned that the exon 9-deleted form of *Tslc1* would not be membrane bound and would lack a functional cytoplasmic domain (splicing of exon 8 with exon 10 would cause a shift in the reading frame). The cytoplasmic domain of TSLC1 (exon 10), containing key protein interaction domains, has been shown to be responsible for its tumor suppressor activities both in vitro and in vivo (27).

The conditional targeting vector was introduced into ES cells, and correctly targeted clones with the genotype $Tslc1^{+/Brdm1}$ (+/*m1*) were identified by Southern blotting (Fig. 1A). +/*m1* ES cell clones were then exposed to either Flpe (to delete the selection cassette) or Cre (to delete both exon 9 and the selection cassette) to generate ES cell lines with the $Tslc1^{+/Brdc1}$ (+/*c1*) and $Tslc1^{+/Brdm2}$ (+/*m2*) alleles, respectively (Fig. 1A). These ES cell clones were used to generate chimeric mice that transmitted the mutated alleles through the germ line. All offspring were genotyped by PCR using the strategy shown in Fig. 1B, which can distinguish between the five possible genotypes (+/+, +/*c1*, *c1*/*c1*, +/*m2*, and *m2*/*m2*).

Interbreeding of heterozygous (+/*c1* or +/*m2*) mice produced homozygous conditional (*c1*/*c1*) and null (*m2*/*m2*) offspring at the expected Mendelian ratios. These mice were indistinguishable from littermate controls in terms of growth and development and did not show decreased survival or an increased incidence of spontaneous tumor development compared to wild-type mice (by 1 year of age). To confirm that the mutant allele was null, RT-PCR was performed on RNAs extracted from the brains of wild-type and homozygous (*m2*/*m2*) mutant mice. Using primers designed against exons 9 and 10, the expected 245-bp product was produced from RNAs from wild-type and *c1*/*c1* mice but not from *m2*/*m2* mice (Fig. 1C and data not shown). Using primers designed against exons 7 to 10, RNAs from wild-type mice produced the expected 291- and 207-bp products (reflecting the alternative isoform of murine *Tslc1* that differs by the 84 bp that constitute exon 8), whereas RNAs from *m2*/*m2* mice produced 159- and 75-bp products (Fig. 1C) which, when sequenced, showed splicing of exon 8 (or exon 7) with exon 10. The skipping of exon 9 in the *m2* allele results in a reading frame shift which is predicted to result in a nonsense transcript. Immunohistochemistry using anti-Tslc1 antibodies on *m2*/*m2* testis sections showed the absence of any Tslc1 protein, in contrast to wild-type testis sections (Fig. 1D). Thus, we concluded that the $Tslc1^{Brdm2}$ allele is null.

***Tslc1* is essential for normal male fertility.** Adult *c1*/*c1* mice were viable, healthy, and fertile, and thus the *c1* allele was not characterized further. However, the conditional inactivation of *Tslc1* using *c1*/*c1* mice will make it possible to evaluate the role of *Tslc1* in specific tissues.

In contrast, although adult *Tslc1* null (*m2*/*m2*) mice appeared normal, no offspring ever resulted from matings between 2- to 3-month-old males and wild-type or *Tslc1* heterozygous females (Table 1). Older *Tslc1* null males (6 to 12 months of age) also showed no evidence of fertility (data not shown), suggesting that a delay in sexual maturation was not the cause of the earlier infertility. A defect in fertility was not observed in *Tslc1* heterozygous males (Table 1), and despite *Tslc1* expression being detected in oocytes (see Fig. S1A in the supplemental material), *Tslc1* null females showed no overt abnormalities in their ovaries (see Fig. S1B in the supplemental material) and possessed fecundity comparable to that of wild-type mice (data not shown). To further investigate the basis for infertility in *Tslc1* null males, spermatozoa were isolated from the caudal regions of *Tslc1* mice at 3 months of age. As shown in Table 1, *Tslc1* null males showed significantly reduced sperm

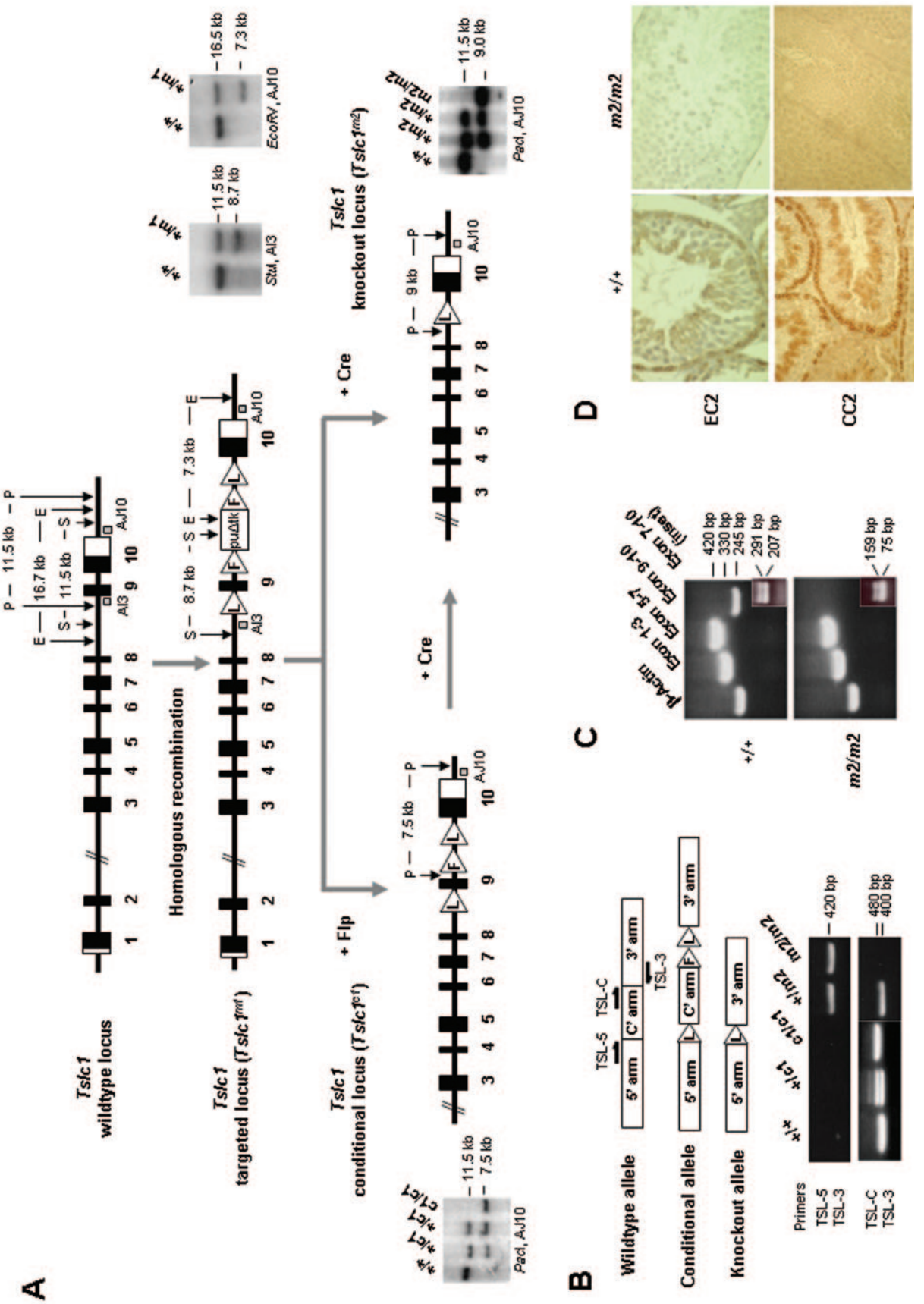
A
Tslc1 wildtype locus
Homologous recombination
Tslc1 targeted locus (Tslc1tm1)
+ Flp
+ Cre
+ Cre
Tslc1 conditional locus (Tslc1tc1)
Tslc1 knockout locus (Tslc1m2)
P — 11.5 kb — P
E — 16.7 kb — E
S — 11.5 kb — S
AI3
AJ10
S — 8.7 kb — S E — 7.3 kb — E
puΔtk
P — 7.5 kb — P
P — 9 kb — P
1 2 3 4 5 6 7 8 9 10
StuI, AI3
EcoRV, AJ10
PacI, AJ10
11.5 kb
8.7 kb
16.5 kb
7.3 kb
9.0 kb
7.5 kb
B
Wildtype allele
Conditional allele
Knockout allele
TSL-5
TSL-C
TSL-3
5' arm
C' arm
3' arm
Primers
TSL-5 TSL-3
TSL-C TSL-3
420 bp
480 bp
400 bp
C
β-Actin
Exon 1-3
Exon 3-7
Exon 9-10
Exon 7-10 (Tsc1)
420 bp
330 bp
245 bp
291 bp
207 bp
159 bp
75 bp
+/+
m2/m2
D
+/+
m2/m2
EC2
CC2

FIG. 1. Generation of null and conditional alleles of *Tslc1*. (A) Tumor suppressor of lung cancer 1 (*Tslc1*) is a 10-exon gene. *loxP* (L) sites were positioned to allow Cre-mediated excision of the transmembrane domain (exon 9) to generate a knockout (null) allele. The *loxP*-flanked genomic segment is located between nucleotide positions 47,952,177 and 47,953,164 on chromosome 9 of Ensembl (NCBI Mouse Genome Assembly m33). The *puroΔtk* cassette, flanked by *FRT* (F) sites, can be excised by using Flp to generate a conditional allele. Southern blot analysis of the *Tslc1* targeted (*m1*), null (*m2*), and conditional alleles (*c1*) was performed using two probes, pAI3 and pAJ10, which are 5′ and 3′ of the targeted allele, respectively. Restriction enzyme sites and fragment sizes are indicated. E, EcoRV; P, PacI; S, StuI. (B) Genotyping of *Tslc1* null and conditional tail DNAs was performed by PCR using a combination of two primer pairs (either TSL-5/TSL-3 or TSL-C/TSL-3) which can distinguish between all five genotypes (+/+, +/*c1*, *c1*/*c1*, +/*m2*, and *m2*/*m2*) based on the presence and size of the product(s), which can be resolved in a 2% agarose gel. (C) RT-PCR was performed to confirm deletion of the *loxP*-flanked exons in *Tslc1* null mice. RT-PCR performed on RNAs extracted from wild-type mice showed a 245-bp product corresponding to *Tslc1* exons 9 and 10. In contrast, no such product was seen for RNAs from *m2*/*m2* mice. RNA from wild-type mice showed 291- and 207-bp products corresponding to exons 7 to 10 and 8 to 10 (reflecting the alternative isoform of murine *Tslc1* that differs by the 84 bp that constitute exon 8), whereas RNA from *m2*/*m2* mice produced 159- and 75-bp products, reflecting the deletion of exon 9. β-*actin* was used as a positive control for cDNA production. (D) Immunohistochemistry performed on testis sections from 3-month-old wild-type and *m2*/*m2* mice, using antibodies against the extracellular domain (EC2) and the C-terminal tail (CC2) of TSLC1.

TABLE 1. Characteristics of sperm from mice with indicated *Tslc1* genotypes

Parameter	Value for mice with indicated genotype		
	+/+	+/*m2*	*m2*/*m2*
Sperm count (10^6/cauda)[a,b]	3.9 ± 2.3	4.1 ± 1.0	0.01 ± 0.01
Sperm motility (%)[b]	50 ± 11	44 ± 21	Rare[c]
Fertility	6/6	15/15	0/15

[a] Sperm count is defined as the number of cells containing a head and a tail.
[b] Counts were obtained from four or five mice per genotype. Data are means ± standard deviations.
[c] Only two motile sperm (in one of four mice examined) were identified on scanning of the whole slide.

counts compared with their wild-type and heterozygous littermates, and the majority of *Tslc1* null sperm were static. Thus, *Tslc1* is essential for normal spermatogenesis and male fertility. Interestingly, adult *Tslc1* null mice did not show a significantly altered level of testosterone (6.3 ± 2.5 nmol/liter; $n = 10$) compared with their wild-type (9.5 ± 4.2 nmol/liter; $n = 9$) or *Tslc1* heterozygous (8.3 ± 5.6 nmol/liter; $n = 4$) littermates; however, this was most likely due to the fact that testosterone is produced by the Leydig cells, which do not express Tslc1 (47) and do not show any abnormalities in *Tslc1* null mice.

Loss of *Tslc1* causes a maturation defect at the spermatid stage of spermatogenesis. Spermatogenesis is a highly organized series of events, with germ cells progressing through multiple phases of development. Histological analysis of sectioned testes and epididymides from *Tslc1* null mice revealed major abnormalities in spermatogenesis. As shown in Fig. 2A, adult testes from wild-type mice at 3 months of age showed spermatogenic cells in all of the different stages of maturation, from spermatogonia to spermatocyte, spermatid, and, finally, spermatozoa, which then passed into the epididymis (Fig. 2C). In contrast, however, adult *Tslc1* null testes showed a nearly complete block in maturation at the spermatid stage of spermatogenesis, with round and elongated spermatids degenerating, dying, and sloughing off into the lumen (Fig. 2B). The few surviving elongated spermatids that underwent the next step of maturation to form spermatozoa did not complete the normal maturation process; the heads of the sperm were fatter than those seen in wild-type mice, had abnormal shapes, and sometimes had no or only rudimentary tails. These degenerating spermatids and immature/malformed spermatozoa that sloughed off into the lumen were subsequently passively propelled into the epididymis (Fig. 2D). We also noted that several *Tslc1* null testes from mice at 3 months of age showed whole tubules undergoing degeneration, with large vacuoles present (Fig. 2E), and in 5-month-old mice, many tubules showed a complete loss of architecture (Fig. 2F), in contrast to the case in wild-type littermates (Fig. 2G).

To further characterize the stage of the maturation defect in *Tslc1* null testes, we determined the frequency distributions of propidium iodide-stained testicular cells from wild-type and *Tslc1* null mice at 3 months of age (Fig. 2H). Compared to wild-type mice, *Tslc1* null mice showed a lower HC cell peak (elongated spermatids), an increased 4C peak (most pachytene spermatocytes and a few G_1 spermatogonia), and a small increase in the 1C peak (round spermatids). It is possible that failure to complete all stages of maturation may have an effect

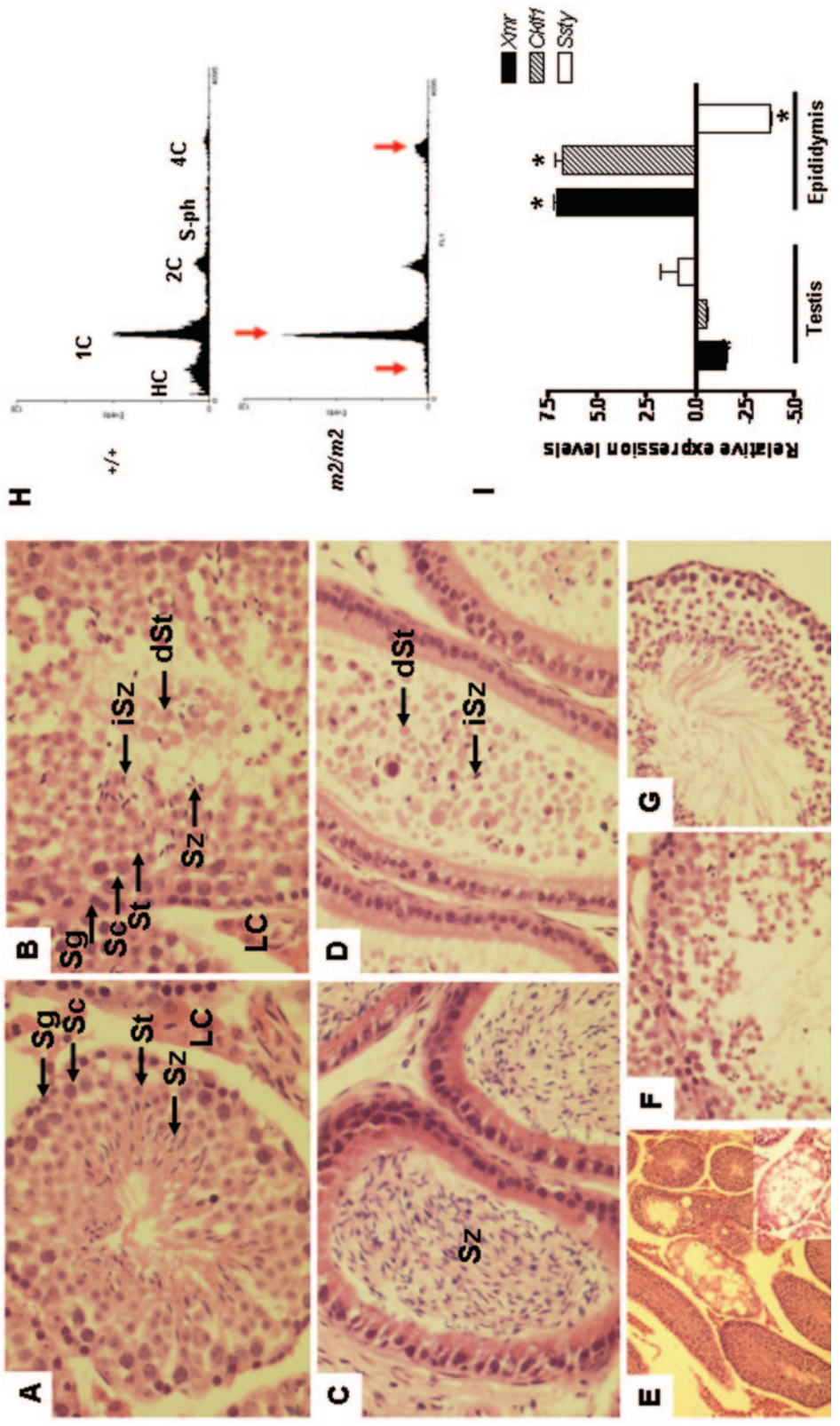

FIG. 2. Analysis of wild-type and *Tslc1* null testes and epididymides. Hematoxylin- and eosin-stained sections of (A) wild-type testis, (B) *Tslc1* null testis, (C) wild-type epididymis, (D) *Tslc1* null epididymis, and (E) *Tslc1* null testis from mice at 3 months of age are shown. Hematoxylin- and eosin-stained testis sections from (F) *Tslc1* null and (G) wild-type mice at 5 months of age are also shown. Magnification, ×400 for panels A to D, ×100 for panels E to G, and ×400 for the inset of panel E. Abbreviations: LC, Leydig cells; Sg, spermatogonia; Sc, spermatocytes; St, spermatids (round and elongated); Sz, spermatozoa; iSz, immature spermatozoa; dSt, degenerated spermatids. (H) DNA flow cytometry analysis of testicular cell suspensions from wild-type and *Tslc1* null (*m2/m2*) mice at 3 months of age ($n = 4$ or 5 for each genotype). Arrows highlight the differences between the wild-type and *Tslc1* null samples. Abbreviations: HC, elongated spermatids; 1C, round spermatids; 2C, spermatogonia; S-ph, spermatogonia synthesizing DNA; 4C, pachytene spermatocytes and G_2 spermatogonia. (I) Real-time quantitative RT-PCR of three spermatid genes, *Ckdf1*, *Xmr*, and *Ssty*, on RNAs extracted from the testes of *Tslc1* null mice at 3 months of age. The results were normalized to β-*actin* and shown as relative changes in expression level compared with the wild type. Asterisks indicate statistical significance in the relative changes in transcript levels between the wild-type and *m2/m2* samples ($P < 0.05$).

(via a feedback mechanism) leading to an increase in cell proliferation of spermatogonia (increased 4C) and then to more spermatocytes (increased 4C) and more round spermatids (increased 1C). Taken together, these observations are consistent with the histological findings of a maturation defect at the spermatid stage with an accumulation of spermatids (mostly round spermatids, with some elongated spermatids) and subsequent degeneration and death of the elongated spermatids with sloughing off into the lumen.

To confirm the origin of the sloughed cells, we carried out real-time quantitative RT-PCR on the transcripts for three known spermatid antigens, namely, *Cklf1* (11), *Xmr* (11), and *Ssty* (8). Both *Cklf1* and *Xmr* were upregulated severalfold in the epididymides of *Tscl1* null males; however, *Ssty* showed a more moderate decrease (Fig. 2I). Since the sloughed cells were positive for *Cklf1* and *Xmr*, this indicates a spermatid origin for these cells. Interestingly, the changes in expression levels of these genes in the testis, though lower in magnitude, are the reverse of the situation in the epididymis, with *Cklf1* and *Xmr* being downregulated and *Ssty* being upregulated. This is consistent with the sloughing of a particular subset of $Cklf1^{+}$ Xmr^{+} $Ssty^{-}$ spermatids into the lumina of the tubules of the testis, with passive propulsion into the epididymis, potentially reflecting stage-specific effects on spermatogenic cell adhesion in *Tscl1* null mice.

***Tslc1* null testes show increased numbers of apoptotic cells.** Adult *Tslc1* null testes from mice at 3 months of age weighed significantly less (0.080 ± 0.003 g; $n = 25$) than testes from their wild-type (0.112 ± 0.004 g; $n = 45$; $P < 0.005$) and *Tslc1* heterozygous (0.105 ± 0.004 g; $n = 27$; $P < 0.005$) littermates, most likely due to the maturation defect at the spermatid stage of spermatogenesis and the degeneration and death of spermatids with sloughing into the lumina of the seminiferous tubules in these mice. To further examine the nature of the spermatid death, we performed TUNEL analysis (Fig. 3). As shown in Fig. 3A, *Tslc1* null testes showed a significantly increased number of TUNEL-positive tubules (tubules containing TUNEL-positive cells; $P < 0.01$), confirming apoptosis as the major mode of cell death. The number of TUNEL-positive cells per TUNEL-positive tubule was also higher in *Tslc1* null testes (Fig. 3B), but this difference was not statistically significant. Interestingly, in contrast with wild-type testes, in which apoptosis occurred in a stage-specific manner and was almost exclusively limited to the spermatogonia (3, 4, 17), *Tslc1* null testes also showed apoptosis occurring in the spermatids (Fig. 3C), thus demonstrating that the increased apoptosis was occurring among the maturation-delayed cells in a non-stage-specific manner. The apoptotic death of cells was also confirmed by electron microscopic examination of the *Tslc1* null testes (data not shown).

Delayed maturation in the first wave of spermatogenesis in juvenile *Tslc1* null mice. In order to unveil the mechanism of maturation arrest of spermatogenesis in *Tslc1* null mice, the progression of the first wave of spermatogenesis was examined in wild-type and *Tslc1* null (*m2*/*m2*) mice (Fig. 4). At postnatal day 7, the histological appearances of the testes from both wild-type and *m2*/*m2* mice were similar, with seminiferous tubules containing only Sertoli cells and spermatogonia. On day 14, when the premeiosis phase of spermatogenesis begins, germ cell differentiation to spermatocytes (primary and secondary) in *m2*/*m2* mice was similar to that seen in wild-type mice. On day 22, the tubules from wild-type and +/*m2* mice that had completed the first and second rounds of meiosis showed the presence of spermatids (mostly round spermatids). However, in *m2*/*m2* mice, progression was delayed, and the most advanced germ cells were primarily still in the late pachytene spermatocyte stage (occasional tubules showed the presence of round spermatids). On day 28, the tubules in most wild-type and +/*m2* mice had completed meiosis, and numerous round and elongated spermatids could be seen, as well as spermatozoa. However, while *m2*/*m2* tubules showed differentiation of the spermatocytes into round spermatids and some elongated spermatids, there was evidence of spermatids degenerating and sloughing off into the lumen. On day 35, tubules from wild-type mice showed the presence of numerous fully matured spermatozoa. In contrast, although the *m2*/*m2* tubules did show the presence of some spermatozoa, they were immature and malformed, with fat or deformed heads and no or only rudimentary tails. Interestingly, many testes from mice on days 22, 28, and 35 showed the presence of multinucleate giant cells (MNC), containing multiple nuclei within a single cytoplasm, suggesting that one feature of degeneration could be the opening up of cytoplasmic bridges between sister spermatids.

***Tslc1* null testes show some features of differentiation.** We next examined *Tslc1*-deficient spermatogenic cells for evidence of certain features of differentiation. Staining of spermatids for glycoproteins showed the presence of an acrosome cap in both wild-type and *Tslc1* null testes in round and elongated spermatids as well as on immature spermatozoon-like head structures in the *Tslc1* null testes (Fig. 5A and B); this finding was confirmed by electron microscopy (data not shown). Since TSLC1 has been shown to directly associate with the F-actin binding protein DAL-1 (49), and since cytoskeletal elements at the Sertoli cell-spermatid interface play critical roles during spermatogenesis (24, 34), we wanted to examine whether the loss of *Tslc1* would result in abnormal actin bundling. However, as shown in Fig. 5C and D, there was no detectable difference in the polarization of F-actin in spermatids from wild-type or *Tscl1* null mice.

***Tslc1* null spermatozoa show major structural abnormalities.** Analysis of the contents of the epididymides from wild-type and *Tslc1* heterozygous (+/*m2*) mice showed mature spermatozoa with their distinctive nuclear morphology (head region), very little cytoplasm, and a tail (Fig. 6A and B, respectively). In stark contrast, the epididymal contents of *Tslc1* null (*m2*/*m2*) mice showed degenerating round spermatids with very few spermatozoa, all of which showed major structural abnormalities, including deformed and irregularly shaped heads, often with a large amount of residual cytoplasm (Fig. 6C to J). Consistent with this, electron microscopy performed on testis sections from wild-type mice showed sperm heads with narrow nuclei and very little surrounding cytoplasm (Fig. 6K). In contrast, sperm heads from *m2*/*m2* mice showed multiple defects, including enlarged nuclei, abnormally shaped nuclei (many of which were degenerated), and large amounts of residual cytoplasm, often with residual body-like changes with dilated mitochondria and vacuoles, suggesting a lack of separation of the residual body from the developing spermatozoa (Fig. 6L to P). MNC with multiple, often abnormally shaped and enlarged, nuclei within a single cellular cytoplasm were also noted (Fig. 6Q and R).

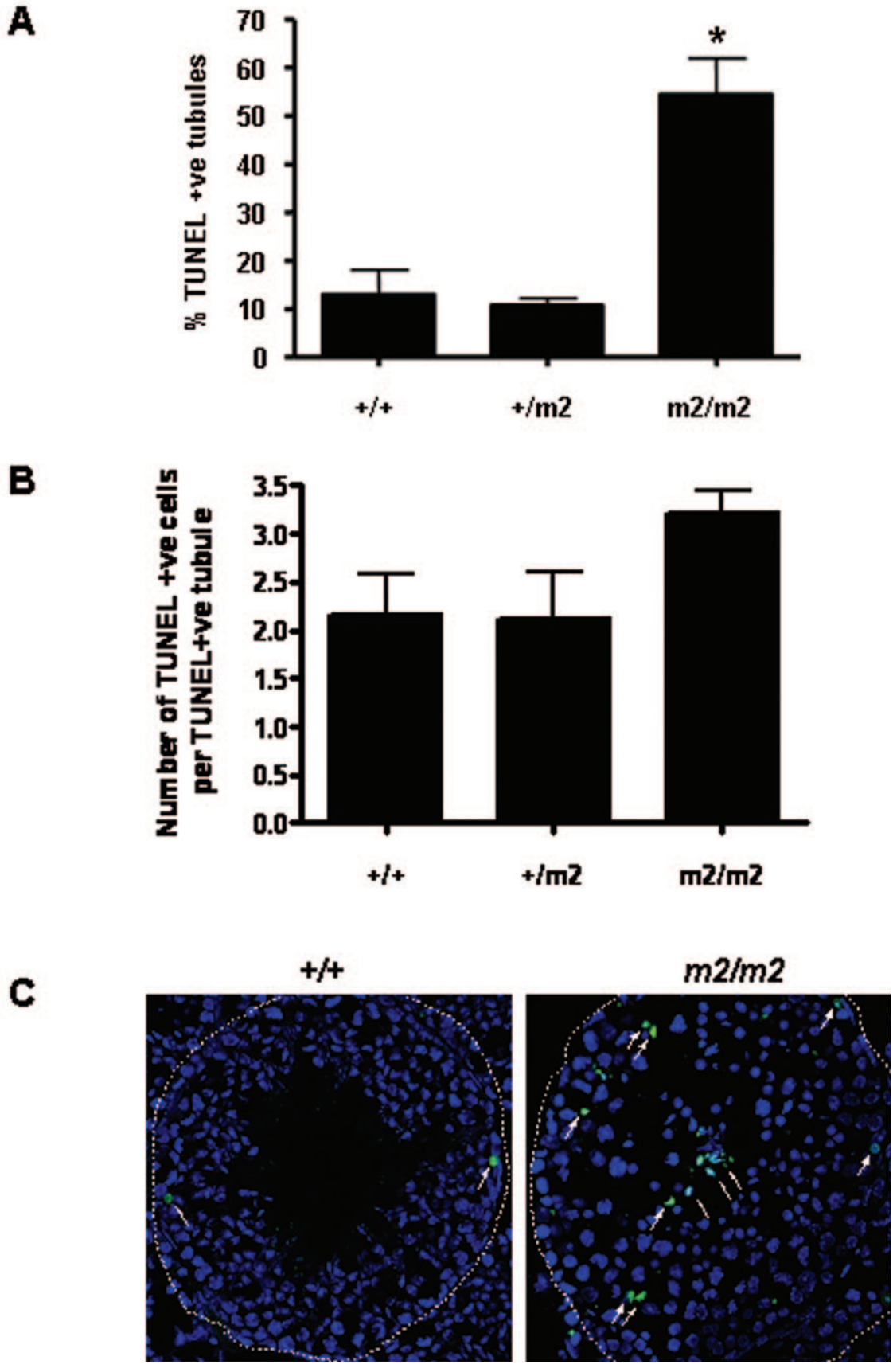
A
% TUNEL +ve tubules
70
60
50
40
30
20
10
0
*
+/+
+/m2
m2/m2
B
Number of TUNEL +ve cells per TUNEL+ve tubule
3.5
3.0
2.5
2.0
1.5
1.0
0.5
0.0
+/+
+/m2
m2/m2
C
+/+
m2/m2

***Tslc1* null testes show upregulated expression of genes involved in apoptosis, adhesion, and the cytoskeleton.** To understand the molecular consequences of the loss of *Tslc1* expression in the testis, we analyzed RNAs from *Tslc1* null testes on a germ cell-specific microarray. The data set was normalized and filtered to select differentially expressed genes, with 136 genes being selected as significantly altered in expression (see Materials and Methods). Interestingly, there were many more upregulated genes (103/136) than downregulated genes, which may reflect the accumulation of transcriptionally active round spermatids and the loss of comparatively transcriptionally inactive elongating spermatids and spermatozoa (Fig. 7; see Table S1 in the supplemental material). Differentially expressed genes were then classified according to their likely biological functions, using Onto-Express (10, 23). As shown in Fig. 7, there was an upregulation of a number of proapoptotic genes, again in agreement with the histological findings of increased spermatid apoptosis. There was also an upregulation of several genes with functions related to the cytoskeleton, cell/cell adhesion, and/or maintaining cell junctions. There was no clear functional bias among downregulated genes. When the differentially expressed genes were compared to previous data (11; unpublished data from the same laboratory [E. Clemente, personal communication]) in order to determine their likely sites of expression, it was found that the majority of these genes appeared to be germ cell specific, with only 10 showing expression profiles suggestive of Sertoli cell expression. This may indicate that the majority of downstream effects of *Tscl1* loss are germ cell specific or may simply reflect the lower abundance of Sertoli cells in whole testicular tissue. One-third of the upregulated genes were expressed in spermatids, consistent with the histological findings of a maturation defect with an accumulation of spermatids (although this upregulation involved only a subset of spermatid-specific genes), whereas downregulated genes showed no clear bias towards different cell types.

DISCUSSION

In multicellular organisms, cells recognize their neighboring cells and adhere to them, forming intercellular junctions that play essential roles in numerous cellular processes (reviewed in reference 20). Furthermore, these intercellular junctions are usually associated with the actin cytoskeleton, which serves to strengthen intercellular adhesion. The seminiferous epithelium of the testis contains two types of intercellular junctions: Sertoli cell-Sertoli cell junctions and Sertoli cell-spermatid junctions (SspJ) (37). Sertoli cells are organized as a single-layered epithelium which cultivates spermatogenic cells throughout spermatogenesis. During the latter half of this process, known as spermiogenesis, spermatids form prominent heterotypic intercellular junctions with Sertoli cells (SspJs), which disappear as the spermatids are released as spermatozoa. These intercellular junctions are formed by cell adhesion molecules on the surfaces of the cells, many of which belong to the IGSF, and a loss of these interactions at these junctions can lead to defects in spermatogenesis. For example, nectin-2 on the surfaces of Sertoli cells interacts with nectin-3 on the surfaces of spermatids, and *nectin-2*-deficient male mice are infertile due to aberrant morphogenesis and positioning of spermatids and severe spermatozoan malformation (6, 32, 34). Similarly, junctional adhesion molecule C (JAM-C) on the surfaces of spermatids binds to JAM-B on the surfaces of Sertoli cells, and *Jam-C*-deficient male mice are infertile due to a failure of round spermatids to differentiate into spermatozoa (18).

TSLC1 (also known as IGSF4, SgIGSF, SynCAM, and Necl-2) is strongly expressed on the surfaces of spermatogenic cells of the seminiferous tubules, but not on Sertoli cells (47). Thus, TSLC1 has been hypothesized to function as a cell adhesion molecule during the early half of spermatogenesis by forming heterotypic intercellular junctions with a membrane molecule on Sertoli cells. In this study, we have generated a *Tslc1* null and a *Tslc1* conditional mouse in order to dissect the role of *Tslc1* in spermatogenesis. We show that *Tslc1* null male mice are infertile due to a maturation defect at the spermatid stage of spermatogenesis. In adult *Tslc1* null mice, this defect is histologically characterized by round (and some elongated) spermatids prematurely degenerating and undergoing apoptosis, sloughing off into the lumen, and then appearing in the epididymis. *Tslc1* null mice show a delay in spermatogenesis in developing testes by day 22, when the most highly differentiated germ cells in the testes are still at the late pachytene spermatocyte stage, and testes at day 28 show round spermatids (and some elongated spermatids) together with degenerating and dying spermatids that slough off into the lumen, akin to what is seen in adult testes. Apoptosis was shown to be the major mode of spermatid death by histology, electron microscopy, and TUNEL staining. This phenotype is similar in mice deficient in nectin-2 and Jam-C (6, 18, 32, 34); both of these proteins play a role in maintaining SspJs, suggesting that the main feature of *Tslc1* loss is a disruption of SspJs.

The histological results were confirmed by flow cytometric analysis of the frequency distributions of propidium iodide-stained testicular cells from adult *Tslc1* null mice. This showed a lower percentage of elongated spermatids and a small increase in the percentage of round spermatids. The relative increase in spermatids seen in *Tslc1* null mice compared to their wild-type littermates could be due to increased spermatid production, possibly indicating a feedback effect from spermatids regulating spermatogonial proliferation and differentiation. Alternatively, the increase in spermatid number may simply reflect a failure to differentiate further into elongating

FIG. 3. *Tslc1* null testes show increased numbers of apoptotic cells. *Tslc1* null (*m2*/*m2*) mice show a statistically significant increase in the percentage of TUNEL-positive tubules compared with wild-type (+/+) mice (as indicated by the asterisk; $P < 0.05$) (A) but not in the number of TUNEL-positive cells per TUNEL-positive tubule (B). (C) Detection of apoptosis (TUNEL-positive cells are indicated by arrows) in testis sections from wild-type mice at 3 months of age, with apoptosis occurring in the spermatogonia, in contrast to *Tslc1* null mice, which show apoptosis occurring in the spermatids as well as the spermatogonia. Slides for three mice of each genotype were examined, and representative slides are shown. Magnification, ×480.

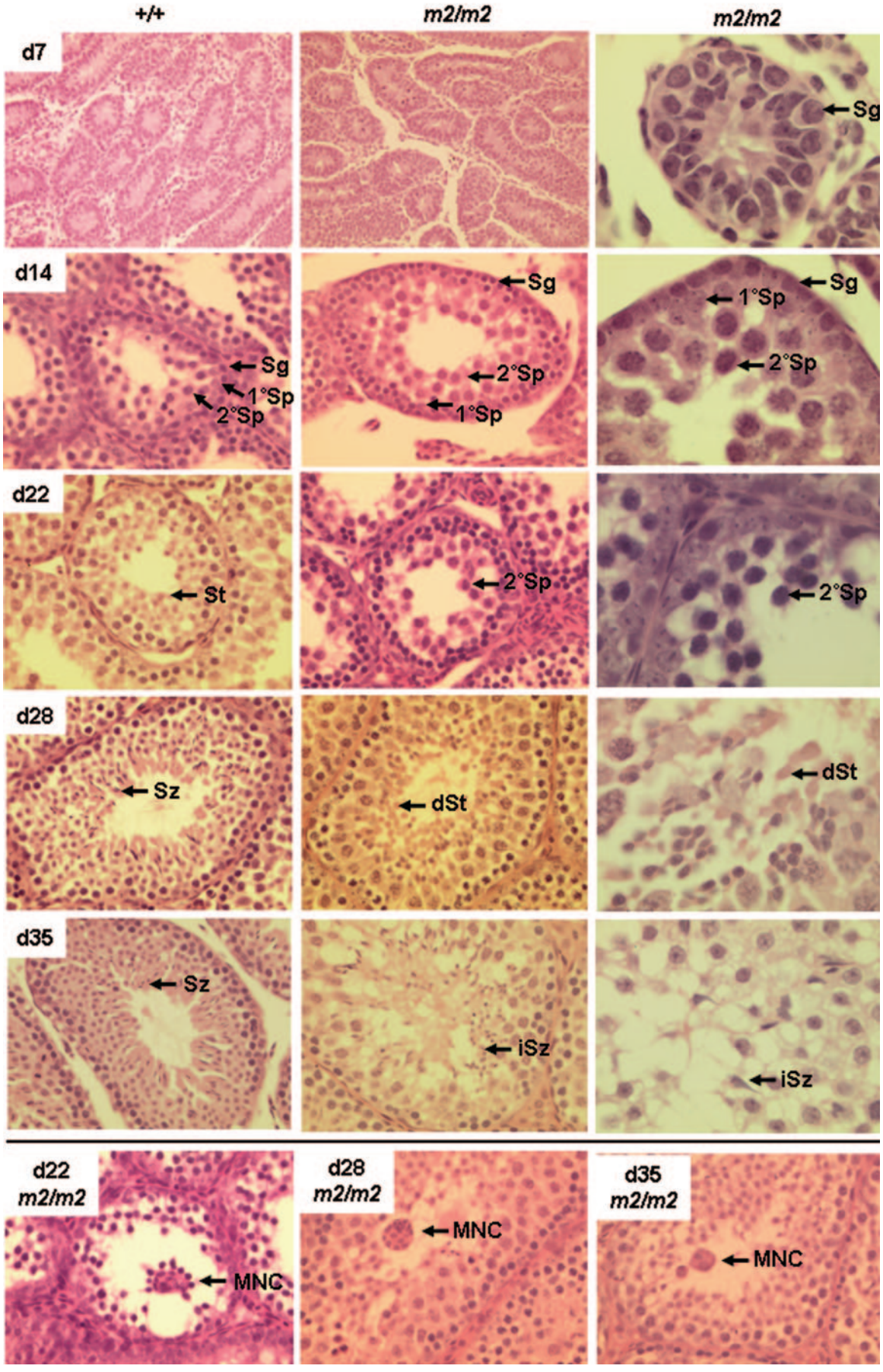
+/+
m2/m2
m2/m2
d7
Sg
d14
Sg
1°Sp
2°Sp
Sg
2°Sp
1°Sp
Sg
1°Sp
2°Sp
d22
St
2°Sp
2°Sp
d28
Sz
dSt
dSt
d35
Sz
iSz
iSz
d22
m2/m2
MNC
d28
m2/m2
MNC
d35
m2/m2
MNC

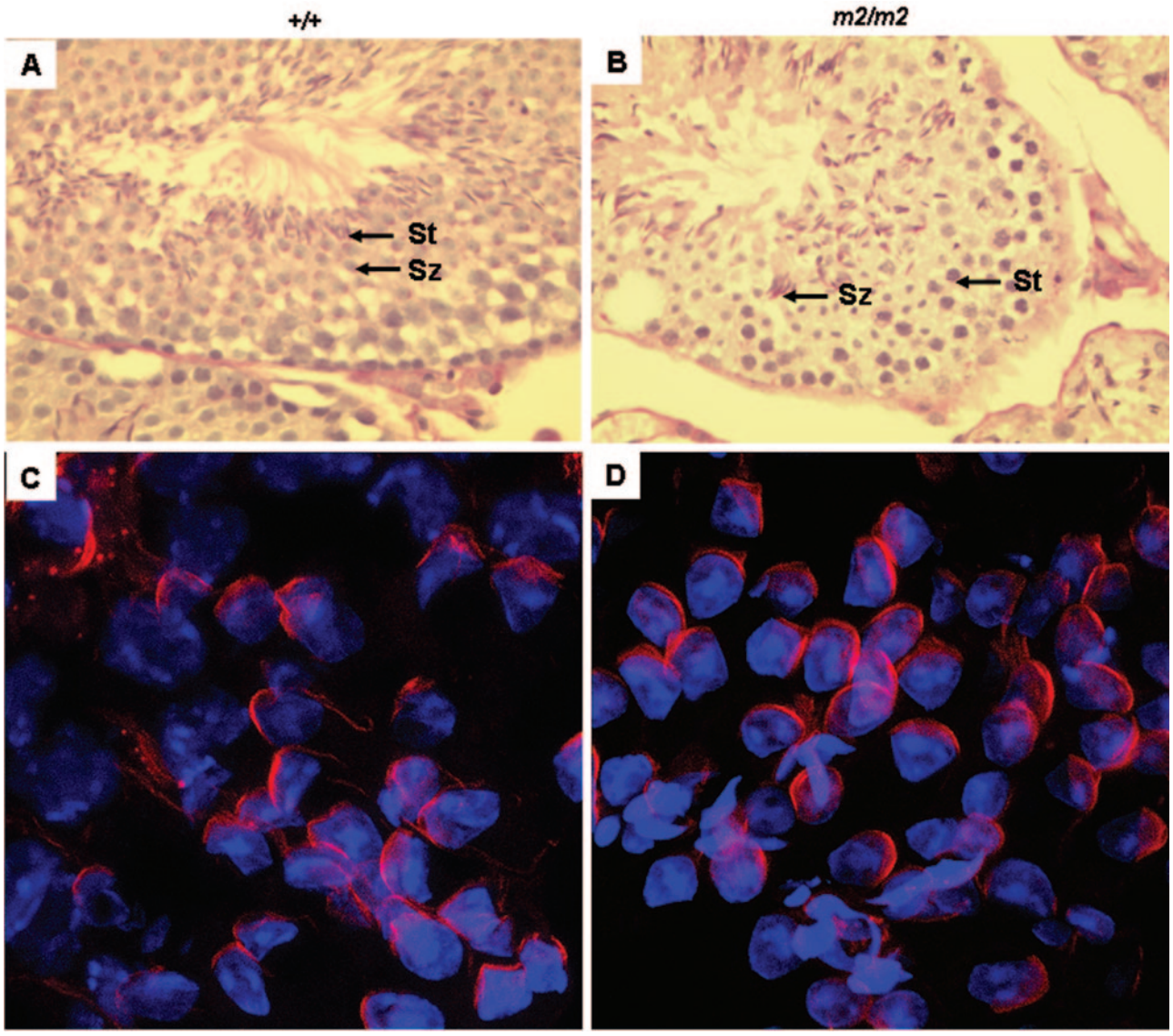

FIG. 5. *Tslc1* null testes show some features of differentiation. Histochemical analysis of testis sections from (A) wild-type and (B) *Tslc1* null (*m2*/*m2*) mice by periodic acid and Schiff staining showed the presence of acrosomal caps (stained pink) in the spermatids (St) and spermatozoa (Sz). Slides for three mice of each genotype were examined, and representative images are shown. Magnification, ×400. An analysis of testis sections from (C) wild-type and (D) *Tslc1* null (*m2*/*m2*) mice by phalloidin staining showed normal F-actin (red) polarization in the spermatids of both. Slides for three mice of each genotype were examined, and representative images are shown. Magnification, ×1,600.

spermatids, with a consequent accumulation of round spermatids.

During normal spermiogenesis, the round spermatids elongate, condense their nuclei, acquire flagellar and acrosomal structures, and shed a significant amount of their cytoplasm (as residual bodies) to form spermatozoa (7). Defects in these processes lead to a lack of mature spermatozoa (azoospermia), which is a major cause of male infertility in the human population (12). While the round spermatids that were present in the adult *Tslc1* null testis showed some hallmarks of normal differentiation, such as the development of an acrosomal cap and normal F-actin polarization, they mostly failed to develop further into elongating spermatids, presumably due to a disruption or loss of normal contact with the Sertoli cell. How-

FIG. 4. Delayed and disrupted first wave of spermatogenesis in *Tslc1* null mice. Hematoxylin- and eosin-stained sections of testes from wild-type (+/+) and *Tslc1* null (*m2*/*m2*) mice at postnatal days 7, 14, 22, 28, and 35 are shown. Magnification for first and second columns, ×200 for day 7 images and ×400 for day 14 to 35 images; magnification for third column, ×1,000. Abbreviations: Sg, spermatogonia; 1° Sp, primary spermatocytes; 2° Sp, secondary spermatocytes; St, spermatids (round and elongated); dSt, degenerated spermatids; Sz, spermatozoa; iSz, immature spermatozoa; MNC, multinucleate giant cells (seen in *m2*/*m2* mice on days 22, 28, and 35; shown at a ×400 magnification).

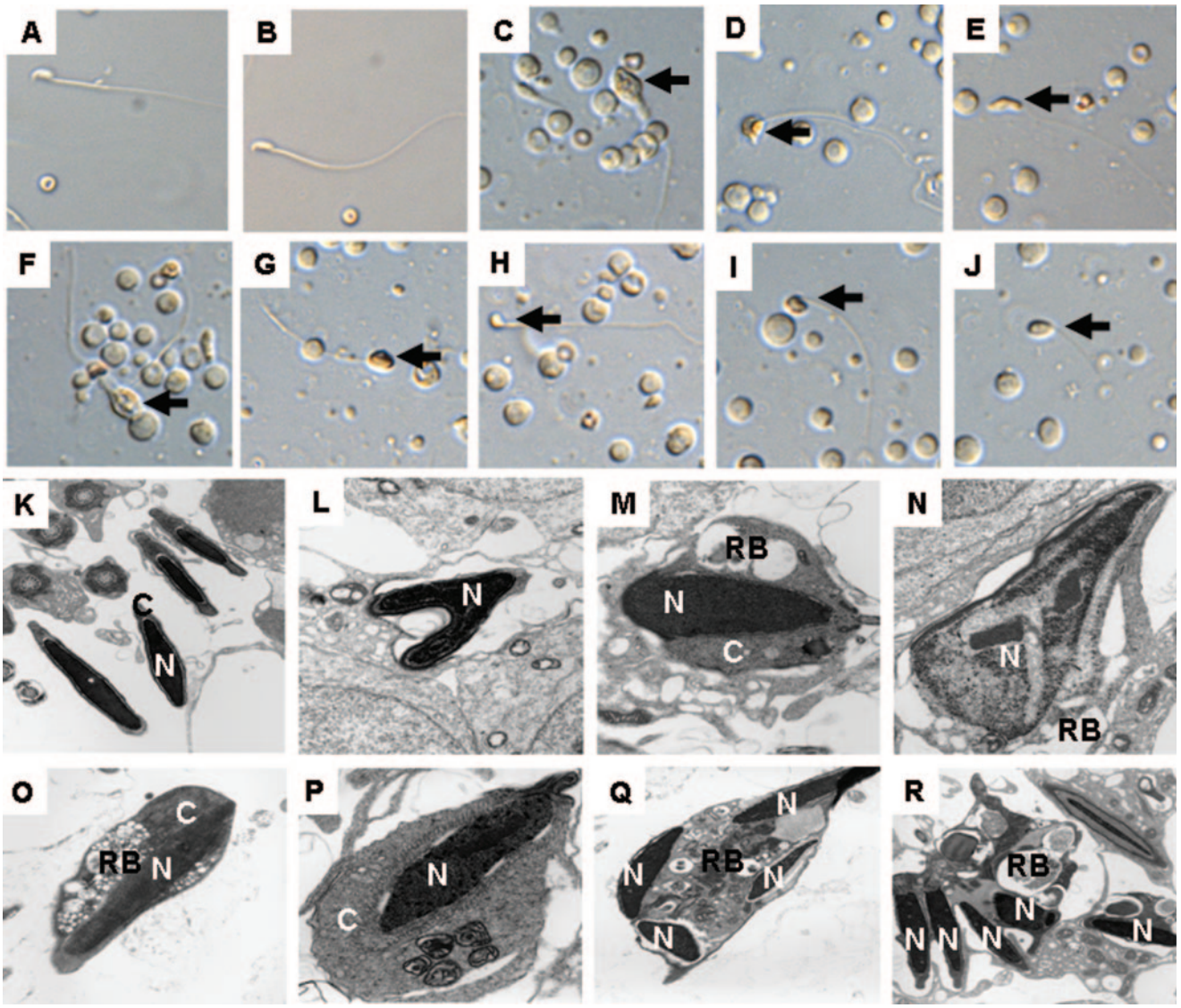

FIG. 6. Analysis of wild-type and *Tslc1* null spermatozoa. Phase-contrast light microscopy showed that in contrast to wild-type (A) or *Tslc1* heterozygous (B) spermatozoa, *Tslc1* null spermatozoa showed morphological abnormalities, as indicated by the arrows (C to J). Images shown are representative of spermatozoa from the caudal epididymides of three to five mice of each genotype. Magnification, ×400. Electron microscopy analysis showed normal sperm head nuclei from wild-type mice (K), in contrast to sperm heads from *Tslc1* null mice, which showed abnormally shaped nuclei (L) and enlarged nuclei with abnormal residual cytoplasm, often showing residual body-like changes (M and O), degenerated nuclei (N), dilated mitochondria and vacuoles (P), and multiple malformed nuclei within a single cellular cytoplasm (Q and R). Abbreviations: N, nucleus; C, cytoplasm; RB, residual body-like changes. Sections from two mice of each genotype were examined, and representative images are shown. Magnification, ×4,500 for panels K to N, Q, and R and ×10,000 for panels O and P.

ever, histological examination showed that the spermatid defect seen in *Tslc1* null mice is not a complete arrest, as a few cells were able to progress to the elongated spermatid stage and then form spermatozoa. Consistent with a defect in spermiogenesis, *Tslc1* null spermatozoa are immature and have larger-diameter heads and no or only rudimentary tails. An analysis of the epididymal contents of *Tslc1* null mice showed these immature/malformed sperm to be found at only very low levels, and rarely were any motile forms detected. Electron microscopy revealed that they had severe head malformations and abnormal amounts of cytoplasm, often with residual body-like changes, including dilated mitochondria and vacuoles. Sperm head abnormalities have also been reported for *nectin-2* null mice (32).

Interestingly, electron microscopy also showed the presence of multiple malformed sperm head nuclei within a single cellular cytoplasm. These MNC were first seen in the developing testis at day 22. This suggests that one feature of the degeneration is the opening up of the cytoplasmic bridges between sister spermatids. However, multinucleate giant cells have also been seen in the developing testes of testicular orphan nuclear receptor 4 (*TR4*) null mice (which are infertile), and it was speculated that they may have resulted from spermatocytes with meiosis defects (31). Similarly, multinucleate degenerated

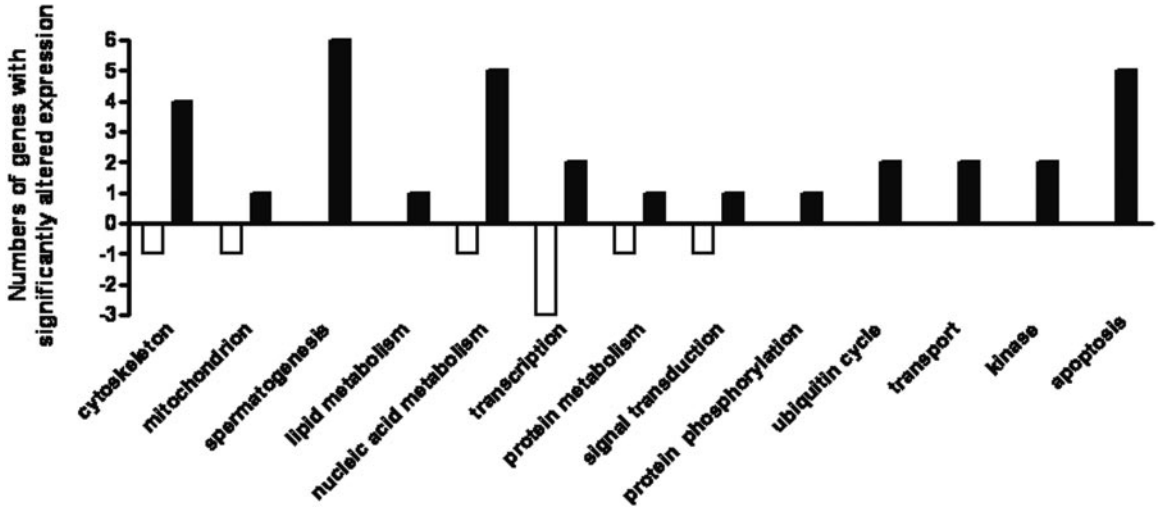

FIG. 7. Microarray analysis of testis RNAs from *Tslc1* null mice. Germ cell-specific microarray analysis was used to identify differentially expressed genes in the testes of *Tslc1* null mice compared with those of wild-type mice. The data set was normalized and filtered to select differentially expressed genes, with 136 genes being selected as significantly altered in expression in *Tslc1* null testes relative to wild-type testes (see Materials and Methods). There were many more upregulated genes (103/136) than downregulated genes, and the differentially expressed genes are shown by classification according to their likely biological function in Onto-Express.

spermatids were also seen in blind-sterile (*bs*) mice (40) and *Bax* null mice (25) and thus may be a nonspecific feature of spermatid degeneration. Alternatively, and more intriguingly, it may be that *Tslc1* has a role in maintaining the integrity of spermatid-spermatid interactions as well as the adherens junctions between the Sertoli cells and spermatids (SspJs).

We were able to discover transcriptional correlates for all of the histological, flow cytometry, and electron microscopy findings via microarray and quantitative RT-PCR analysis. Transcription profiling confirmed the expansion in spermatid numbers, with one-third of the upregulated genes being known or putative spermatid transcripts. However, this upregulation did not apply to all spermatid transcripts on the array, suggesting that the increase in spermatid number is due to the expansion of a particular subset of the spermatid population. Functional classification of the deregulated genes showed upregulation of a number of proapoptotic factors and also of genes with putative roles in cytoskeletal function and/or cell adhesion. This reflects the apoptosis and degeneration seen in the expanded spermatid population and the failure of these cells to undergo normal morphological differentiation into elongating spermatids and, subsequently, spermatozoa. Intriguingly, despite the severe failure in the development of late-stage structures such as the sperm tail, there was no corresponding loss of transcripts involved in the production of these structures, suggesting that much of the transcriptional program involved in spermatid differentiation is able to continue despite the failure of the morphological program of differentiation.

Sloughing of degenerating spermatids was confirmed by quantitative RT-PCR, which showed upregulated expression of the spermatid-specific genes *Xmr* and *Cklf1* in the epididymis and a consequent slight downregulation of these genes in the testis due to cell loss. Thus, the overall transcriptional picture in the testis is complex, with upregulation of some spermatid genes due to the net expansion in round spermatid numbers but downregulation of other spermatid genes due to cell sloughing. Further analysis of the transcriptional changes (in particular, an in situ examination of transcript localization) will clarify which spermatid stages are retained and expanded in the mutant testis and which are lost through cell sloughing and degeneration. In particular, such analysis should help to reveal which elements of the spermatid differentiation program are innate and which are dependent upon Sertoli cell contact.

Based on the data presented here, we hypothesize that Tslc1 expressed by spermatogenic cells binds to an unknown heterophilic partner on Sertoli cells to mediate a functionally important cell-cell interaction involving transmission of survival and differentiation signals. The loss of Tslc1 does not appear to affect early spermatogenic development (spermatogonia to spermatocytes), possibly because there is no real need for adhesion molecules to maintain close contact between these cell types and the supporting Sertoli cells, as they are already held in place by the latter (due to their physical location within the tubule). It is only when there is a possibility of being shed into the lumen, as occurs at the spermatid stage, that cell adhesion molecules play a critical role in maintaining tight Sertoli cell-spermatid contact. It is in the last steps of spermatogenesis that elongated spermatids are considered to undergo active surface interaction with Sertoli cells in the process of displacement of the spermatid cytoplasm from the condensing nuclei, its casting off as a residual body, and subsequent phagocytosis by the Sertoli cells (13). The major impact of the loss of Tslc1 is in the late stage of spermatogenesis (elongated spermatids to spermatozoa) and underscores this protein's vital role in cell-cell interactions, particularly between elongated spermatids and Sertoli cells at SspJs. It seems feasible that genetic defects, as well as other factors interfering with normal TSLC1 function in the reproductive system, could lead to male infertility in humans.

ACKNOWLEDGMENTS

L.V.D.W. and D.J.A. are recipients of Australian NHMRC postdoctoral research fellowships (C. J. Martin/R. G. Menzies Fellowship and C. J. Martin Fellowship, respectively). M.J.A. is supported by Cancer Research UK. This research was supported by the Wellcome Trust and the BBSRC.

We thank Daisuke Yamada for immunohistochemistry experiments, Midori Yoshida for assistance with histopathological analysis, Anthony Brown and David Carter for cDNA microarray production and quality control, Emily Clemente for input in statistical analysis of the microarray experiments and discussions of microarray results, Beverly Haines and Graham Gatward for assistance with histology and electron microscopy, Joanna Maldonado-Saldivia for the oocyte (germinal vesicle stage) cDNA library, Evelyn Grau and Tina Hamilton for microinjection of the targeted ES cell lines, and the personnel of Team 83 for care and monitoring of the animals.

REFERENCES

1. **Arends, M. J., R. G. Morris, and A. H. Wyllie.** 1990. Apoptosis: the role of the endonuclease. Am. J. Pathol. **136:**593–608.
2. **Biederer, T., Y. Sara, M. Mozhayeva, D. Atasoy, X. Liu, E. T. Kavalali, and T. C. Sudhof.** 2002. SynCAM, a synaptic adhesion molecule that drives synapse assembly. Science **297:**1525–1531.
3. **Blanco-Rodriguez, J.** 1998. A matter of death and life: the significance of germ cell death during spermatogenesis. Int. J. Androl. **21:**236–248.
4. **Blanco-Rodriguez, J., C. Martinez-Garcia, and A. Porras.** 2003. Correlation between DNA synthesis in the second, third and fourth generations of spermatogonia and the occurrence of apoptosis in both spermatogonia and spermatocytes. Reproduction **126:**661–668.
5. **Boles, K. S., W. Barchet, T. Diacovo, M. Cella, and M. Colonna.** 2005. The tumor suppressor TSLC1/NECL-2 triggers NK cell and CD8+ T cell responses through the cell surface receptor CRTAM. Blood **106:**779–786.
6. **Bouchard, M. J., Y. Dong, B. M. McDermott Jr., D. H. Lam, K. R. Brown, M. Shelanski, A. R. Bellve, and V. R. Racaniello.** 2000. Defects in nuclear and cytoskeletal morphology and mitochondrial localization in spermatozoa of mice lacking nectin-2, a component of cell-cell adherens junctions. Mol. Cell. Biol. **20:**2865–2873.
7. **Cheng, C. Y., and D. D. Mruk.** 2002. Cell junctions dynamics in the testis: Sertoli germ cell interactions and male contraceptive development. Physiol. Rev. **82:**825–874.
8. **Conway, S. J., S. K. Mahadevaiah, S. M. Darling, B. Capel, A. M. Rattigan, and P. S. Burgoyne.** 1994. Y353/B: a candidate multiple-copy spermiogenesis gene on the mouse Y chromosome. Mamm. Genome **5:**203–210.
9. **de Kretser, D. M., T. Meehan, M. K. O'Bryan, N. G. Wreford, R. I. McLachlan, and K. L. Loveland.** 2000. Regulatory mechanisms in mammalian spermatogenesis, p. 87–106. *In* B. Jegou, C. Pineau, and J. Saez (ed.), Testis, epididymus and technologies in the year 2000. Springer-Verlag, Berlin, Germany.
10. **Draghici, S., P. Khatri, R. P. Martins, G. C. Ostermeier, and S. A. Krawetz.** 2003. Global functional profiling of gene expression. Genomics **81:**98–104.
11. **Ellis, P. J., R. A. Furlong, A. Wilson, S. Morris, D. Carter, G. Oliver, C. Print, P. S. Burgoyne, K. L. Loveland, and N. A. Affara.** 2004. Modulation of the mouse testis transcriptome during postnatal development and in selected models of male infertility. Mol. Hum. Reprod. **10:**271–281.
12. **Ezeh, U. I.** 2000. Beyond the clinical classification of azoospermia: opinion. Hum. Reprod. **15:**2356–2359.
13. **Fawcett, D. W.** 1975. Ultrastructure and function of the Sertoli cell, p. 21–55. *In* D. W. Hamilton and R. O. Greep (ed.), Handbook of physiology, vol. 5. American Physiological Society, Baltimore, Md.
14. **Fujita, E., A. Soyama, and T. Momoi.** 2003. RA175, which is the mouse ortholog of TSLC1, a tumor suppressor gene in human lung cancer, is a cell adhesion molecule. Exp. Cell Res. **287:**57–66.
15. **Fukuhara, H., M. Masuda, M. Yageta, T. Fukami, M. Kuramochi, T. Maruyama, T. Kitamura, and Y. Murakami.** 2003. Association of a lung tumor suppressor TSLC1 with MPP3, a human homologue of Drosophila tumor suppressor Dlg. Oncogene **22:**6160–6165.
16. **Galibert, L., G. S. Diemer, Z. Liu, R. S. Johnson, J. L. Smith, T. Walzer, M. R. Comeau, C. T. Rauch, M. F. Wolfson, R. A. Sorensen, A. R. Van der Vuurst de Vries, D. G. Branstetter, R. M. Koelling, J. Scholler, W. C. Fanslow, P. R. Baum, J. M. Derry, and W. Yan.** 2005. Nectin-like protein 2 defines a subset of T-cell zone dendritic cells and is a ligand for class-I-restricted T-cell-associated molecule. J. Biol. Chem. **280:**21955–21964.
17. **Giampietri, C., S. Petrungaro, P. Coluccia, A. D'Alessio, D. Starace, A. Riccioli, F. Padula, S. M. Srinivasula, E. Alnemri, F. Palombi, A. Filippini, E. Ziparo, and P. De Cesaris.** 2003. FLIP is expressed in mouse testis and protects germ cells from apoptosis. Cell Death Differ. **10:**175–184.
18. **Gliki, G., K. Ebnet, M. Aurrand-Lions, B. A. Imhof, and R. H. Adams.** 2004. Spermatid differentiation requires the assembly of a cell polarity complex downstream of junctional adhesion molecule-C. Nature **431:**320–324.
19. **Gomyo, H., Y. Arai, A. Tanigami, Y. Murakami, M. Hattori, F. Hosoda, K. Arai, Y. Aikawa, H. Tsuda, S. Hirohashi, S. Asakawa, N. Shimizu, E. Soeda, Y. Sakaki, and M. Ohki.** 1999. A 2-Mb sequence-ready contig map and a novel immunoglobulin superfamily gene IGSF4 in the LOH region of chromosome 11q23.2. Genomics **62:**139–146.
20. **Gumbiner, B. M.** 1996. Cell adhesion: the molecular basis of tissue architecture and morphogenesis. Cell **84:**345–357.
21. **Hynes, R. O.** 1999. Cell adhesion: old and new questions. Trends Cell Biol. **9:**M33–M37.
22. **Kargul, G. J., D. B. Dudekula, Y. Qian, M. K. Lim, S. A. Jaradat, T. S. Tanaka, M. G. Carter, and M. S. Ko.** 2001. Verification and initial annotation of the NIA mouse 15K cDNA clone set. Nat. Genet. **28:**17–18.
23. **Khatri, P., S. Draghici, G. C. Ostermeier, and S. A. Krawetz.** 2002. Profiling gene expression using onto-express. Genomics **79:**266–270.
24. **Kierszenbaum, A. L., E. Rivkin, and L. L. Tres.** 2003. Acroplaxome, an F-actin-keratin-containing plate, anchors the acrosome to the nucleus during shaping of the spermatid head. Mol. Biol. Cell **14:**4628–4640.
25. **Knudson, C. M., K. S. Tung, W. G. Tourtellotte, G. A. Brown, and S. J. Korsmeyer.** 1995. Bax-deficient mice with lymphoid hyperplasia and male germ cell death. Science **270:**96–99.
26. **Kuramochi, M., H. Fukuhara, T. Nobukuni, T. Kanbe, T. Maruyama, H. P. Ghosh, M. Pletcher, M. Isomura, M. Onizuka, T. Kitamura, T. Sekiya, R. H. Reeves, and Y. Murakami.** 2001. TSLC1 is a tumor-suppressor gene in human non-small-cell lung cancer. Nat. Genet. **27:**427–430.
27. **Mao, X., E. Seidlitz, K. Ghosh, Y. Murakami, and H. P. Ghosh.** 2003. The cytoplasmic domain is critical to the tumor suppressor activity of TSLC1 in non-small cell lung cancer. Cancer Res. **63:**7979–7985.
28. **Masuda, M., M. Yageta, H. Fukuhara, M. Kuramochi, T. Maruyama, A. Nomoto, and Y. Murakami.** 2002. The tumor suppressor protein TSLC1 is involved in cell-cell adhesion. J. Biol. Chem. **277:**31014–31019.
29. **McCarrey, J. R., D. A. O'Brien, and M. K. Skinner.** 1999. Construction and preliminary characterization of a series of mouse and rat testis cDNA libraries. J. Androl. **20:**635–639.
30. **McMahon, A. P., and A. Bradley.** 1990. The Wnt-1 (int-1) proto-oncogene is required for development of a large region of the mouse brain. Cell **62:**1073–1085.
31. **Mu, X., Y. F. Lee, N. C. Liu, Y. T. Chen, E. Kim, C. R. Shyr, and C. Chang.** 2004. Targeted inactivation of testicular nuclear orphan receptor 4 delays and disrupts late meiotic prophase and subsequent meiotic divisions of spermatogenesis. Mol. Cell. Biol. **24:**5887–5899.
32. **Mueller, S., T. A. Rosenquist, Y. Takai, R. A. Bronson, and E. Wimmer.** 2003. Loss of nectin-2 at Sertoli-spermatid junctions leads to male infertility and correlates with severe spermatozoan head and midpiece malformation, impaired binding to the zona pellucida, and oocyte penetration. Biol. Reprod. **69:**1330–1340.
33. **Murakami, Y.** 2005. Involvement of a cell adhesion molecule, TSLC1/IGSF4, in human oncogenesis. Cancer Sci. **96:**543–552.
34. **Ozaki-Kuroda, K., H. Nakanishi, H. Ohta, H. Tanaka, H. Kurihara, S. Mueller, K. Irie, W. Ikeda, T. Sakai, E. Wimmer, Y. Nishimune, and Y. Takai.** 2002. Nectin couples cell-cell adhesion and the actin scaffold at heterotypic testicular junctions. Curr. Biol. **12:**1145–1150.
35. **Quackenbush, J.** 2002. Microarray data normalization and transformation. Nat. Genet. **32**(Suppl.)**:**496–501.
36. **Ramirez-Solis, R., P. Liu, and A. Bradley.** 1995. Chromosome engineering in mice. Nature **378:**720–724.
37. **Russell, L. D., and M. D. Griswold.** 1993. The Sertoli cell. Cache River Press, Vienna, Ill.
38. **Schaft, J., R. Ashery-Padan, F. van der Hoeven, P. Gruss, and A. F. Stewart.** 2001. Efficient FLP recombination in mouse ES cells and oocytes. Genesis **31:**6–10.
39. **Shingai, T., W. Ikeda, S. Kakunaga, K. Morimoto, K. Takekuni, S. Itoh, K. Satoh, M. Takeuchi, T. Imai, M. Monden, and Y. Takai.** 2003. Implications of nectin-like molecule-2/IGSF4/RA175/SgIGSF/TSLC1/SynCAM1 in cell-cell adhesion and transmembrane protein localization in epithelial cells. J. Biol. Chem. **278:**35421–35427.
40. **Sotomayor, R. E., and M. A. Handel.** 1986. Failure of acrosome assembly in a male sterile mouse mutant. Biol. Reprod. **34:**171–182.
41. **Takeichi, M.** 1988. The cadherins: cell-cell adhesion molecules controlling animal morphogenesis. Development **102:**639–655.
42. **Tanaka, T. S., S. A. Jaradat, M. K. Lim, G. J. Kargul, X. Wang, M. J. Grahovac, S. Pantano, Y. Sano, Y. Piao, R. Nagaraja, H. Doi, W. H. Wood III, K. G. Becker, and M. S. Ko.** 2000. Genome-wide expression profiling of mid-gestation placenta and embryo using a 15,000 mouse developmental cDNA microarray. Proc. Natl. Acad. Sci. USA **97:**9127–9132.
43. **Tseng, G. C., M. K. Oh, L. Rohlin, J. C. Liao, and W. H. Wong.** 2001. Issues in cDNA microarray analysis: quality filtering, channel normalization, models of variations and assessment of gene effects. Nucleic Acids Res. **29:**2549–2557.
44. **Van Buren, V., Y. Piao, D. B. Dudekula, Y. Qian, M. G. Carter, P. R. Martin, C. A. Stagg, U. C. Bassey, K. Aiba, T. Hamatani, G. J. Kargul, A. G. Luo, J. Kelso, W. Hide, and M. S. Ko.** 2002. Assembly, verification, and initial annotation of the NIA mouse 7.4K cDNA clone set. Genome Res. **12:**1999–2003.

45. **van der Weyden, L., D. J. Adams, L. W. Harris, D. Tannahill, M. J. Arends, and A. Bradley.** 2005. Null and conditional semaphorin 3B alleles using a flexible puroΔtk LoxP/FRT vector. Genesis **41:**171–178.
46. **Wakayama, T., K. Ohashi, K. Mizuno, and S. Iseki.** 2001. Cloning and characterization of a novel mouse immunoglobulin superfamily gene expressed in early spermatogenic cells. Mol. Reprod. Dev. **60:**158–164.
47. **Wakayama, T., H. Koami, H. Ariga, D. Kobayashi, Y. Sai, A. Tsuji, M. Yamamoto, and S. Iseki.** 2003. Expression and functional characterization of the adhesion molecule spermatogenic immunoglobulin superfamily in the mouse testis. Biol. Reprod. **68:**1755–1763.
48. **Watabe, K., A. Ito, Y. I. Koma, and Y. Kitamura.** 2003. IGSF4: a new intercellular adhesion molecule that is called by three names, TSLC1, SgIGSF and SynCAM, by virtue of its diverse function. Histol. Histopathol. **18:**1321–1329.
49. **Yageta, M., M. Kuramochi, M. Masuda, T. Fukami, H. Fukuhara, T. Maruyama, M. Shibuya, and Y. Murakami.** 2002. Direct association of TSLC1 and DAL-1, two distinct tumor suppressor proteins in lung cancer. Cancer Res. **62:**5129–5133.
50. **Yagi, T., S. Nada, N. Watanabe, H. Tamemoto, N. Kohmura, Y. Ikawa, and S. Aizawa.** 1993. A novel negative selection for homologous recombinants using diphtheria toxin A fragment gene. Anal. Biochem. **214:**77–86.